Oxygen and nitric oxide rebinding kinetics in nonsymbiotic hemoglobin AHb1 from Arabidopsis thaliana

ARTICLE *in* INTERNATIONAL UNION OF BIOCHEMISTRY AND MOLECULAR BIOLOGY LIFE · DECEMBER 2011

Impact Factor: 3.14 · DOI: 10.1002/iub.546 · Source: PubMed

8 AUTHORS, INCLUDING:

Stefania Abbruzzetti
Università degli studi di Parma
75 PUBLICATIONS **1,392** CITATIONS
SEE PROFILE

Francesca Spyrakis
Università degli Studi di Modena e Reggio E…
61 PUBLICATIONS **1,098** CITATIONS
SEE PROFILE

Stefano Bruno
Università degli studi di Parma
76 PUBLICATIONS **1,197** CITATIONS
SEE PROFILE

Andrea Mozzarelli
Università degli studi di Parma
215 PUBLICATIONS **5,020** CITATIONS
SEE PROFILE

IUBMB *Life*, 63(12): 1094–1100, December 2011

Research Communication

Oxygen and Nitric Oxide Rebinding Kinetics in Nonsymbiotic Hemoglobin AHb1 from *Arabidopsis thaliana*

Stefania Abbruzzetti[1,2],* Serena Faggiano[3], Francesca Spyrakis[4], Stefano Bruno[3], Andrea Mozzarelli[3], Alessandra Astegno[2], Paola Dominici[2] and Cristiano Viappiani[1,5]

[1]*Dipartimento di Fisica, Università degli Studi di Parma, Parma, Italy*
[2]*Dipartimento di Biotecnologie, Università degli Studi di Verona, Verona, Italy*
[3]*Dipartimento di Biochimica e Biologia Molecolare, Università degli Studi di Parma, Parma, Italy*
[4]*Dipartimento di Chimica Generale ed Inorganica, Chimica Analitica, Chimica Fisica, Università degli Studi di Parma, Parma, Italy, and INBB, Istituto Nazionale Biostrutture e Biosistemi, Consorzio Interuniversitario, Rome, Italy*
[5]*NEST, Istituto Nanoscienze-CNR, Italy*

Summary

Type 1 nonsymbiotic hemoglobin from *Arabidopsis thaliana* (AHb1) shows a partial bis-histidyl hexacoordination but can reversibly bind diatomic ligands. The physiological function is still unclear, but the high oxygen affinity rules out a function related to O_2 sensing, carrying, or storing. To gain insight into its possible functional roles, we have investigated its O_2 and NO rebinding kinetics after laser flash photolysis. The rate constants of the rebinding from the primary docking site for both O_2 and NO are higher than CO, with lower photolysis yields. Moreover, the amplitude of the geminate phase increases and, as for CO, the numerical analysis of the experimental curves suggests the existence of an internal pathway leading, with high rate, to an additional docking site. However, the accessibility to this site seems to be strongly ligand-dependent, being lower for O_2 and higher for NO.
IUBMB *Life*, 63(12): 1094–1100, 2011

Keywords hemeproteins; hemoglobin; nitric oxide.

INTRODUCTION

In plants, there are three phylogenetic classes of nonsymbiotic hemoglobins (nsHbs), so named because they are not associated with bacteria-mediated nitrogen fixation. Their properties were recently reviewed (*1–3*). NsHb AHb1 from *Arabidopsis thaliana* belongs to class 1 nsHbs and is expressed under several conditions of stress, including hypoxia and nitric oxide exposure (*4, 5*). AHb1 combines an extremely high O_2 affinity, ($K_d \approx 2$–10 nM) with an internal hexacoordination of the distal histidine, HisE7, in the absence of external ligands. The very high oxygen affinity, due to a very low dissociation rate constant, means that AHb1 strongly stabilizes O_2 after binding, thus ruling out a possible function related to O_2 sensing, carrying, or storing (*6*), whereas a role in electron transport is unlikely because of its high redox potential (*7, 8*). As suggested in general for class 1 nsHbs (*9*), and proved *in vivo* for maize and alfalfa lines overexpressing class 1 nsHbs (*8, 10*), AHb1 may participate in NO detoxification by acting as NO scavenger under hypoxic stress. In fact, the rapid nitrate accumulation from the reaction of oxyAHb1 with NO *in vitro* may be physiologically relevant *in vivo* to reduce the levels of NO under hypoxic stress (*11, 12*).

It is generally accepted that type 1 nsHbs play a role in a metabolic pathway involving NO, which may provide an alternative type of respiration to mitochondrial electron transport under limiting oxygen concentrations (*2, 13*). Experimental evidence indicates that under hypoxic conditions AHb1 and other type 1 nsHbs act as part of a soluble, terminal, NO dioxygenase system, yielding nitrate from the reaction of oxyHb with NO (*9, 11, 14*).

In analogy with neuroglobin (*15*), a system of hydrophobic cavities, potentially capable of temporarily stocking reactants and/or products was proposed to be central to sustain the turnover of this enzymatic activity in class 1 nsHbs. Indeed, migration of diatomic gases in the internal cavities of the protein was experimentally demonstrated for AHb1 (*16–19*), and the possible pathways identified by computational studies (*20*).

In particular, we have suggested that access of NO to the heme cavity could be facilitated in the oxygenated state, as binding of

Received 10 February 2011; accepted 2 July 2011
Address correspondence to: Stefania Abbruzzetti, Dipartimento di Fisica, Università degli Studi di Parma, Parco Area delle Scienze, 7/A, Parma 43124, Italy. Tel: +39-052-190-5208. Fax: +39-052-190-5223. E-mail: stefania.abbruzzetti@fis.unipr.it
Present address of Serena Faggiano: MRC National Institute for Medical Research, The Ridgeway, Mill Hill, London NW7 1AA, United Kingdom.

ISSN 1521-6543 print/ISSN 1521-6551 online
DOI: 10.1002/iub.546

O_2 to the heme iron would trigger the opening of a gate connecting the distal site to the solvent through a secondary cavity, allowing the migration of NO as an incoming ligand from the solvent (*20*), or involving the formation of a Cys-NO adduct (*11*).

In most studies, CO was used as a model ligand, given the well-known experimental advantages of using this gas over O_2 and NO. However, it seems important to evaluate the reactivity of O_2 and NO, the physiological ligands for the NO dioxygenase activity, with the protein, and to assess their mobility through the internal cavities. In this work, we report results from nanosecond laser flash photolysis on O_2 and NO complexes with ferrous AHb1.

EXPERIMENTAL PROCEDURES

AHb1 was cloned, expressed, and purified as described elsewhere. (*17*) For flash photolysis experiments on NOAHb1, a 100-mM potassium phosphate solution buffered at pH 7.4 and deoxygenated through nitrogen bubbling was used to anaerobically dissolve methylamine hexamethylene methylamine NONOate powder (MAHMA NONOate, Cayman Chemical) to give a final concentration of 2 mM. Separately, a solution 35-μM deoxyAHb1 in phosphate buffer at pH 7.0 was prepared by anaerobically adding aliquots of a sodium dithionite solution until complete reduction was achieved, as monitored by UV–vis spectrophotometry (Cary 4000, Varian). An aliquot of the stock solution of MAHMA NONOate was then added to the AHb1 solution to give a final concentration of 100 μM. Excess NO was finally removed by fluxing nitrogen in a gas-tight cuvette for 30 min. This procedure allowed a better control on the NO concentration of the solution, which was always stoichiometric, inside the holder used for the flash photolysis experiment. The protein was confirmed to have remained in the NO-complexed form by UV–vis spectrophotometry.

For the flash photolysis experiments on oxyAHb1, the Hayashi reagents (*21*) were added to a 100-mM sodium phosphate buffer at pH 7.0, containing AHb1 at a concentration of 73 μM, to protect the protein from autooxidation. The sample, in a gas-tight cuvette endowed with a reservoir, was then equilibrated with either oxygen at 1 atm (for single wavelength experiments) or with a 10% (for time resolved spectral changes) or 20% of oxygen mixture in helium (for single wavelength experiments). For the experiments at stoichiometric concentrations of protein and oxygen, the sample was first equilibrated with air and then fluxed in nitrogen for 30 min.

Flash photolysis was carried out with the circularly polarized second harmonic (532 nm) of a Q-switched Nd: yttrium aluminium garnet (YAG) laser, and a cw Xe arc lamp as a probe source. The transient absorbance traces were measured at 436 nm through a 0.25-m spectrograph with a five-stage photomultiplier. The experimental setup was as described previously (*22, 23*).

The kinetics of O_2 and NO binding after rapid mixing were measured using a thermostated stopped flow apparatus (Applied Photophysics, Salisbury, United Kingdom) with a dead time of about 1 ms. Deoxy AHb1 was prepared reducing oxygenated AHb1 with a stoichiometric amount of Na dithionite, and it was mixed in the stopped flow apparatus with either O_2 (200 μM O_2 after mixing) or NO (70 μM after mixing), at different temperatures between 5 and 25 °C. The concentration of AHb1 was 8 μM after mixing.

$$LHb \underset{k_{-1}}{\overset{h\upsilon}{\rightleftharpoons}} \left(Hb_p : L\right)_1 \underset{k_{-2}}{\overset{k_2}{\rightleftharpoons}} Hb_p + L$$
$$k_{-c} \uparrow\downarrow k_c \qquad k_{-b} \uparrow\downarrow k_b$$
$$\left(Hb_p : L\right)_2 \qquad Hb_h + L$$

Scheme 1. Relevant chemical equilibria for the reaction of ligand (L = CO, O_2, or NO) with AHb1 (*Hb*) to form the liganded species (*LHb*). Pentacoordinated- and hexacoordinated, bis-histidyl species were indicated by the suffix *p* and *h*, respectively. $(Hb_p : L)_1$ indicates primary docking sites with L still inside the distal pocket, while $(Hb_p : L)_2$ indicates a site in which the photodissociated ligand is docked into an internal hydrophobic cavity, accessible from the primary docking site.

Singular value decomposition (SVD) of the time resolved differential absorption spectra was performed within Matlab as described previously (*23*).

We have followed the minimal model previously proposed for AHb1 (*23*) and sketched in Scheme 1 (*vide infra*) to describe the rebinding kinetics. The differential equations associated with Scheme 1 were solved numerically, and the rate constants appearing in the equilibrium were optimized to obtain a best fit simultaneously to the laser flash photolysis and stopped flow data. Numerical solutions to the set of coupled differential equations corresponding to Scheme 1 were determined by using the function ODE15s within Matlab 7.0 (The MathWorks). Fitting of the numerical solution to experimental data (and optimization of microscopic rate constants) was obtained with a Matlab version of the optimization package Minuit Conseil Européen pour la Recherche Nucléaire (CERN).

To improve the retrieval of microscopic rate constants, data from flash photolysis of O_2AHb1 complex at the same temperature but different ligand concentrations (at stoichiometric concentration and equilibrated with 0.2 and 1 atm) were simultaneously fitted. This global analysis was repeated at several different temperatures between 10 and 25 °C.

The global analysis was applied also to fit simultaneously ligand (O_2 and NO) binding kinetics from stopped flow and flash photolysis (which had different ligand concentrations) at the same temperature. The activation parameters for the microscopic rate constants were determined from the resulting linear Eyring plots (see Table 1).

RESULTS AND DISCUSSION

The ferrous form of AHb1 can form stable complexes with O_2, CO, and NO, with absorption spectra similar to those of the corresponding species in human Hb, displaying α and β peaks

Table 1
Microscopic rate constants, activation[a] enthalpies (kcal mol^{-1}), entropies (cal mol^{-1} K^{-1}), and free energies (kcal mol^{-1}) determined for wt AHb1 from the global fit of flash photolysis and stopped flow data at 20 °C

	CO[b]				O_2				NO			
	k	$\Delta S^{\ddagger}$	$\Delta H^{\ddagger}$	$\Delta G^{\ddagger}$	k	$\Delta S^{\ddagger}$	$\Delta H^{\ddagger}$	$\Delta G^{\ddagger}$	k	$\Delta S^{\ddagger}$	$\Delta H^{\ddagger}$	$\Delta G^{\ddagger}$
k_{-1} (10^6 s^{-1})	5.13	−14.0 ± 0.5	–	4.1 ± 0.5	12	−27 ± 1	–	7.9 ± 0.1	100	−21.9 ± 0.1	–	6.5 ± 0.1
k_2 (10^7 s^{-1})	9	−12.9 ± 0.6	2.7 ± 0.1	6.5 ± 0.1	2.0	−11 ± 2	4.1 ± 0.8	7.4 ± 0.8	4.3	−11 ± 5	2 ± 1	6 ± 2
k_{-2} (10^7 M^{-1}s^{-1})	2.26	26 ± 2	14.7 ± 0.6	7.1 ± 0.6	70	−17 ± 1	0.4 ± 0.2	5.3 ± 0.3	30	−11.4 ± 0.1	2.4 ± 0.1	5.8 ± 0.1
k_c (10^7 s^{-1})	2.07	−12.6 ± 0.6	–	3.7 ± 0.6	0.35	−28.5 ± 0.2	–	8.3 ± 0.1	4	−23.7 ± 0.1	–	7.0 ± 0.1
k_{-c} (10^7 s^{-1})	0.25	−14.7 ± 0.5	–	4.3 ± 0.5	0.23	−29.6 ± 0.5	–	8.7 ± 0.1	1.4	−25.8 ± 0.1	–	7.7 ± 0.1
k_b (s^{-1})	23.5	12 ± 4	19 ± 1	15.5 ± 0.9	185	24 ± 8	21 ± 2	14 ± 5	187	5 ± 3	15 ± 3	14 ± 10
k_{-b} (s^{-1})	14.5	8 ± 4	18 ± 1	15.6 ± 0.9	107	20 ± 5	20 ± 1	14 ± 4	110	13 ± 8	18 ± 3	15 ± 10

[a]Activation enthalpies $\Delta H^{\ddagger}$ and entropies $\Delta S^{\ddagger}$ were estimated from Eyring plots for each rate constant k_i in the temperature range 10–40 °C, according to the equation: $\ln\left(\frac{hk_i}{k_B T}\right) = \frac{\Delta S^{\ddagger}}{R} - \frac{\Delta H^{\ddagger}}{RT}$, where R is the gas constant, h is the Planck's constant, and k_B is the Boltzmann constant.
[b]Data from ref. *17*.The reliability of each parameter was proved evaluating the dependence of the squared chi on changes of the parameter, assuming the others as constant. $k_{-1} \approx 15\%$; $k_2 \approx 10\%$; $k_{-2} \approx 4\%$; $k_c \approx 50\%$; $k_{-c} \approx 50\%$; $k_b \approx 3\%$; $k_{-b} \approx 3\%$.

of different intensity (Fig. 1A). The ligand rebinding kinetics following nanosecond laser photolysis of either O_2AHb1 or NOAHb1 solutions were recorded as a function of ligand con-

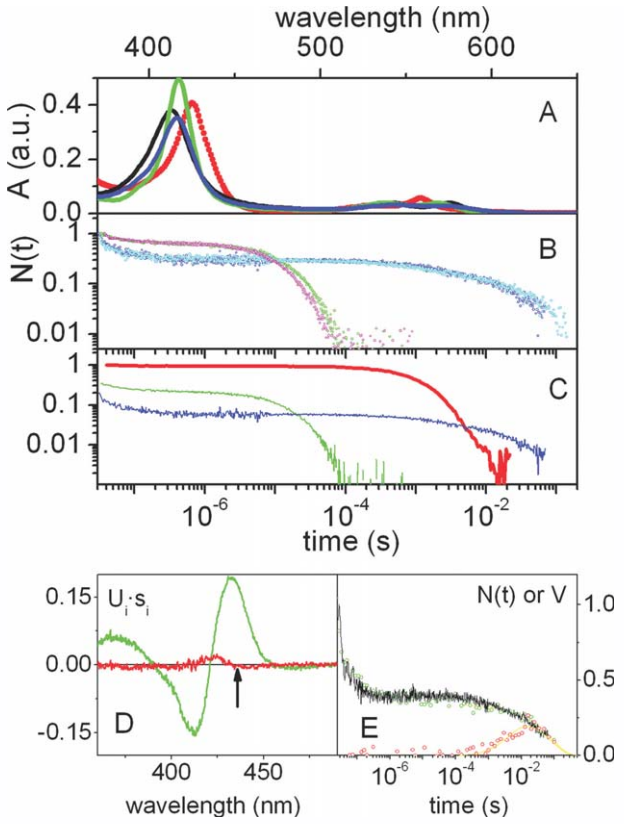

Figure 1. A: UV–vis absorption spectra Fe^{2+}deoxy AHb1 (425 nm, red dotted line) and CO-bound form (417 nm, green line), O_2-bound form (413 nm, black line) and NO-bound form (416 nm, blue line). AHb1 (25.7 μM) is in 100 mM phosphate buffer at pH = 7.0, T = 20 °C. B: Comparison between CO (red line), O_2 (green line) and NO (blue line) rebinding kinetics to ferrous AHb1 solutions. Solutions were equilibrated with 1 atm CO and 1 atm O_2. NO was present in stoichiometric amount. T = 10 μC. Protein concentration was 70–80 μM. C: NO rebinding kinetics to AHb1, at 10 °C (blue) and 25 °C (cyan). O_2 rebinding kinetics, at 10 °C (green) and 25 °C (magenta). 1 atm O_2. D: Comparison of the weighted first ($U_1 \cdot s_1$, green line) and second ($U_2 \cdot s_2$, red lines) spectral components obtained from the SVD analysis on the time-resolved differential absorption spectra measured for NOAHb1 (s_1 = 2.2 and s_2 = 0.18). The arrow in Panel D indicates the wavelength used in single wavelength experiments (436 nm). E: Time courses of the amplitudes V_1 (green open circles) and V_2 (red open circles) obtained for NOAHb1 are superimposed to the single wavelength kinetics at 436 nm (black solid line). NO was present in stoichiometric amount and T was 20 °C. In the figure we have also reported the provisional fits (yellow lines) of the second order phase, obtained from a global analysis of V_1 and V_2 with a sum of two exponential decay functions.

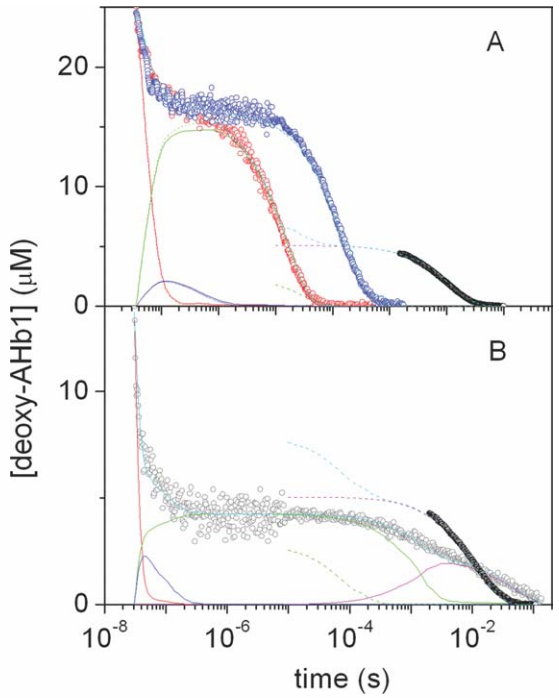

Figure 2. Results of global analysis of O_2 (A) and NO (B) binding kinetics to AHb1 from stopped flow (black circles, (A) 200 μM O_2, (B) 70 μM NO), and laser flash photolysis at 284 μM O_2 (1 atm, red circles) and 57 μM O_2 (0.2 atm, blue circles) and stoichiometric concentration of NO (gray circles), T = 20 °C. The fits (cyan lines) are superimposed to the experimental data (circles). In the figures, we have also reported the time course of the other relevant species in Scheme 1: $(Hb_p{:}L)_1$ (red), $(Hb_p{:}L)_2$ (blue), Hb_h (magenta), and Hb_p (green).

centration and temperature (Figs. 1 and 2) at 436 nm. At this wavelength, the absorbance changes reflect exclusively ligand binding as demonstrated by the SVD analysis of transient absorption spectra, discussed below. In Fig. 1, D and E report the results of the SVD analysis on the time resolved differential absorption spectra measured after photolysis of a NOAHb1 solution. Similar results were obtained for an O_2AHb1 solution, equilibrated with 0.1 atm O_2. Only two meaningful components were retrieved from the analysis, rejecting those with U and V autocorrelations below 0.8, as previously described (*24*). The weighted main component ($U_1{\cdot}s_1$) closely reproduces the deoxy-minus NOAHb1 (or O_2-) difference absorption spectrum, whereas the weighted second component ($U_2{\cdot}s_2$) represents only a minor contribution (a few percent) to the overall spectral change. The second component has a spectral shape, with a clear peak at 425 nm, which is essentially identical to the one we reported earlier for COAHb1, which was attributed to histidine binding to, and dissociation from the heme. (*23*) The time course of the amplitude V_2 demonstrates that the reaction intermediate (the bis-histidyl hexacoordinated species) overlaps in time with the slowest phase in the reaction progress, as reported by V_1 and by the absorbance change at 436 nm.

The negligible amplitude of the weighted second spectral component ($U_2{\cdot}s_2$) at 436 nm means that, at this wavelength, the corresponding amplitude ($U_2{\cdot}s_2{\cdot}V_2$) is zero at all times after photolysis. Thus, the absorbance changes at 436 nm following photolysis are a direct measure of the rebinding kinetics and do not reflect spectral changes associated with distal His binding to, and dissociation from the heme. This can be fully appreciated in Fig. 1E, where the time course of normalized V_1 perfectly overlaps to the absorbance change measured at 436 nm. It should be kept in mind that the time profile of the main SVD component (and, hence, of the absorbance change at 436 nm) only measures the time profile of the concentration of deoxyAHb1, but has a composite kinetics which arises from elementary reaction steps, including geminate recombination, second-order rebinding from the solvent, and binding to and dissociation from the heme of the distal His.

The amplitude V_2 of the second spectral component is essentially zero until almost 0.5 ms, then increases to reach a maximum at about 20 ms, and finally decays with the same kinetics as V_1. The spectral shape $U_2{\cdot}s_2$ and the time profile of the amplitude V_2 clearly demonstrate that the last kinetic phase (in V_1 and in the absorbance change at 436 nm) is associated with formation and decay of the bis-histidyl hexacoordinated species.

The dependence on ligand concentration can be exploited to distinguish between unimolecular and bimolecular rebinding phases, whereas the dependence on temperature gives access to the thermal activation parameters. The absorbance change following photodissociation of COAHb1 is normalized to 1 at the maximum value (reached at the end of the laser pulse), then plotted as a fraction of deoxyhemes present at time t. Figure 1B compares the rebinding kinetics observed after photolysis of the ferrous complexes of AHb1 with CO, O_2, and NO. We have previously observed that the nanosecond photolysis yield measured for COAHb1, using human HbA as a standard, is 1 within the experimental errors (*17*). This parameter measures the fraction of excited molecules which survives as deoxy species at the end of the laser pulse. Through the same comparative method, we have estimated that the nanosecond photolysis yields for O_2 and NO are 0.35 and 0.2, respectively. Accordingly, the fraction of deoxy ferrous AHb1 has different values, determined by the photolysis yields, at the end of the laser pulse, for the three ligands used in this study. While after photolysis only a minor fraction of CO molecules reacts geminately with the heme on the nanosecond time scale, nanosecond geminate rebinding accounts for about 40 and 70% of the signal for O_2 and NO, respectively. The low photolysis yield and the very steep slope in the early nanoseconds suggest that time-resolved experiments with subnanosecond resolution will be necessary to better appreciate the innermost reaction step.

A clear-cut ligand concentration dependence of the kinetic phase in the long microseconds identifies this step as a second-order kinetics (see Fig. 2 for O_2 as a ligand). A comparison

between the O_2- and CO-rebinding kinetics in Fig. 1B immediately shows the enormous increase in the onrate for O_2 in comparison to CO. A direct visual inspection is not possible for NO as the gas is at stoichiometric concentration, and this results in a comparatively slower reaction.

The slowest portion of the rebinding kinetics reflects the formation of a bis-histidyl hexacoordinated species, a process that, in the case of the NOAHb1 complex, leads to a visually very heterogeneous kinetics.

Comparison of the signals at different temperatures in Fig. 1C demonstrates that the temperature has negligible effects on the geminate recombination and induces only small changes in the second-order phase. This was also suggested by previous experiments (*17, 20*), which pointed out that protein fluctuations only slightly affect the migration of the photodissociated CO from the distal pocket of AHb1 to the solvent at near physiological temperatures. This effect, as reported herein, is only slightly dependent on the nature of the diatomic ligand.

Following the approach used to describe the reactivity of AHb1 with CO, we have chosen a minimal model, shown in Scheme 1, which in addition to ligand migration, requires competitive binding between the exogenous (CO, O_2, or NO) and the endogenous (HisE7) ligands (*17, 18*). This model was tested earlier for COAHb1 solutions and proved to describe correctly also NO and O_2 rebinding kinetics (either measured after laser photolysis or rapid mixing) reported herein. The differential equations associated with Scheme 1 were solved numerically, and the microscopic rate constants were optimized using a nonlinear least squares algorithm. A global analysis was performed, where experimental binding curves from flash photolysis and stopped flow at the same temperature were simultaneously fitted. At each temperature, we were able to reproduce the ligand rebinding kinetics with a common set of rate constants at all tested ligand concentrations. Figure 2 reports the results of the kinetic analysis, under selected conditions, of the O_2 and NO binding kinetics.

The rate constants retrieved from the binding curves at 20 °C are reported in Table 1, along with the corresponding activation parameters. The exit of ligands from the heme pocket is easier in the case of CO than for O_2 and NO, as shown by the difference in photolysis yield and geminate amplitude (Fig. 1B). The lower exit probability to the solvent, observed for O_2 and NO, is due to both a decrease in rate k_2 and an increase in rate k_{-1}. In the case of NO, the rate k_{-1} undergoes a dramatic increase (20-fold in comparison with CO). However, independently of the diatomic ligand, geminate rebinding is nonexponential, reflecting at least two kinetic phases, attributed in Scheme 1 to the existence of a second internal docking site.

The rate k_{-1} shows negligible temperature dependence in the investigated temperature range, similarly to what found for CO rebinding to other globins such as myoglobin (*25*), neuroglobin (*26, 27*), human hemoglobin (*28*), and nonsymbiotic rice hemoglobin (*29*). The lower escape probability to the solvent (rate k_2) for O_2 and NO in comparison with CO is reflected in the increase in their respective free energy barriers.

Numerical analysis shows that the experimental curves are consistent with the existence of a pathway leading, with high rate, to an internal docking site, from which the ligand can quickly return to the primary cavity. This process is very weakly temperature dependent, suggesting that the access route to this secondary docking site is open and does not require movements of bulky side chains. However, comparison between the values of k_c reveals that the accessibility to this site is dependent on the nature of the ligand, with the following order: k_c (O_2) < k_c (CO) < k_c (NO). On the other hand, the reverse rate k_{-c} follows a similar order k_c (O_2) ≈ k_c (CO) < k_c (NO). This means that the docking site is quickly populated but then rapidly left free by NO. This can be taken as an indication that NO can be delivered efficiently to the active site, assumed to be the oxygenated ferrous AHb1. It is interesting to compare the present results with those obtained with FTIR combined with temperature derivative spectroscopy at cryogenic temperatures. Under those conditions, it is not possible to trap NO in a secondary docking site in AHb1, unlike the case of CO (*19*). Thus, it appears that protein fluctuations occurring at near physiological temperatures, but inhibited at low temperatures, are necessary for NO migration.

Ligand entry rate into the protein matrix from the solution (rate k_{-2}) has remarkably higher values for O_2 and NO (30- and 15-folds, respectively) with respect to CO. Activation free energies for O_2 and NO are similar and smaller about 2 kcal/mol than CO. This results from smaller activation enthalpies and from activation entropies of small absolute value and opposite sign.

From the data reported in Table 1, we can estimate the binding rate constants to the pentacoordinated specie as $k_{on}(CO) = 1.22 \times 10^6\ M^{-1}\ s^{-1}$, $k_{on}(O_2) = 2.6 \times 10^8\ M^{-1}\ s^{-1}$, and $k_{on}(NO) = 2.5 \times 10^8\ M^{-1}\ s^{-1}$, confirming an increased reactivity of AHb1 for O_2 and NO.

Surprisingly, the kinetic analysis suggests that formation and disappearance of the hexacoordinated, bis-histidyl species occurs in much higher rate when the AHb1 complex with O_2 and NO is photolyzed. In fact, both the binding rate of the distal His to the heme Fe (k_b), and the dissociation rate are higher, by nearly eightfold, than the corresponding values obtained from the analysis of CO rebinding kinetics. While rate constants appear to be higher, the equilibrium constant is ligand independent, being ~ 1.7, as we previously observed in presence of CO.

The source for this remarkably different behavior is as yet unclear. CO, O_2, and NO are diatomic ligands with different physical–chemical properties, which may tune to a different extent protein dynamics during their migration through exchange channels and cavities located inside the protein. This may lead to a different competition between the exogenous ligand and the distal His for binding to the heme iron.

While at this stage, we are unable to propose a molecular mechanism for the observed effects, possible specific interaction with protein residues may be suggested for NO. The structural features of cavities and tunnels potentially involved in the migration of ligands through the protein emerging from

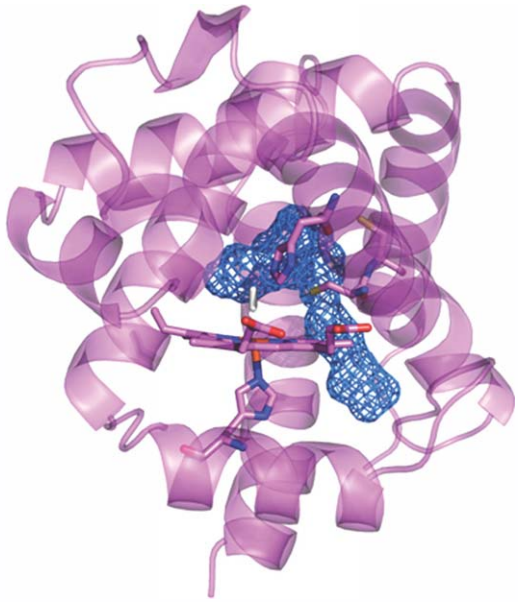

Figure 3. Representation of the tunnel (blue meshed surface) connecting the distal pocket with the solvent bulk identified by FPOCKET, in the protein matrix of the oxygenated model of AHb1. The proximal and the distal histidines, the cysteines located on helix E, and the heme are represented in capped sticks.

extended molecular dynamics simulations (*20*) comprise the presence of a secondary cavity transiently accessible to the bulk solvent through the movement of the side chain of His147 (Fig. 3). This secondary cavity appears to be directly connected to the distal cavity in the oxy state, and only transiently in the 5c-deoxy form through rearrangements of the side chains of residues Cys77, Cys78, Leu121, and mainly Tyr145. NO molecules could be trapped in this cavity close to the heme and then released into the distal pocket. According to the mechanism proposed, it may be suggested that NO migrates inside the protein matrix up to the secondary docking site delineated by some well-defined residues, as Cys77 and Cys78 (E15 and E16). Transient interactions with these and other amino acids lining this secondary cavity may affect the mobility of helix E and bias the competition between the endogenous and exogenous ligand in favor of the former.

Cys77 and Cys78 were previously identified as relevant amino acids in NO involving reactions for AHb1 (*11*). This fact may have interesting functional implications, because AHb1 S-nitrosylation was suggested to take part in the NO-detoxifying activity of AHb1, in analogy with the NO-dependent cysteine-mediated dioxygenase mechanism reported for *Ascaris suum* Hb, having a homologous Cys in position E15. The nematode S-nitrosylated Hb was shown to react with O_2 through the formation of a peroxynitrite intermediate which quickly isomerizes to nitrate, leaving Fe^{3+} heme and a cysteinyl radical, further reduced by NADPH (*30*). Also mammalian Hbs are reported to undergo S-nitrosylation, but the role of this reaction in red blood cells is quite controversial. Stamler and coworkers proposed that the formation of SNO-Hb on human beta-Cys93 through reaction of Hb with nitrite is involved in NO mediated hypoxic vasodilation (*31, 32*). Recent experiments on beta-Cys93 knock-out mice, however, showed that SNO-Hb is not essential for the nitrite-induced vasodilating effect (*33*). In any case, even if related to the exploitation of distinct functions in different organisms (*i.e.*, NO delivery or detoxification, or others), the relevance of Hb S-nitrosylation in NO homeostasis appears clear (*34*).

In this context, future studies addressing specifically the differences in the dynamical behavior of wt AHb1 and its mutant without Cys residues, using NO as a ligand, will help understanding the involvement of Cys residues in modulating heme hexacoordination.

ACKNOWLEDGEMENTS

The authors acknowledge the Italian Ministero dell'Istruzione, dell'Università e della Ricerca (PRIN 2004 2004052135, PRIN 2008, 2008BFJ34R, and Azioni Integrate Italia Spagna 2009) for financial support.

REFERENCES

1. Smagghe, B. J., Hoy, J. A., Percifield, R., Kundu, S., Hargrove, M. S., Sarath, G., Hilbert, J. L., Watts, R. A., Dennis, E. S., Peacock, W. J., Dewilde, S., Moens, L., Blouin, G. C., Olson, J. S., and Appleby, C. A. (2009) Correlations between oxygen affinity and sequence classifications of plant hemoglobins. *Biopolymers* **91**, 1083–1096.
2. Dordas, C. (2009) Nonsymbiotic hemoglobins and stress tolerance in plants. *Plant Sci.* **176**, 433–440.
3. Kakar, S., Hoffman, F. G., Storz, J. F., Fabian, M., and Hargrove, M. S. (2010) Structure and reactivity of hexacoordinate hemoglobins. *Biophys. Chem.*152, 1–14.
4. Trevaskis, B., Watts, R. A., Andersson, C. R., Llewellyn, D. J., Hargrove, M. S., Olson, J. S., Dennis, E. S., and Peacock, W. J. (1997) Two hemoglobin genes in *Arabidopsis thaliana*: the evolutionary origins of leghemoglobins. *Proc. Natl. Acad. Sci. USA* **94**, 12230–12234.
5. Wang, R., Guegler, K., LaBrie, S. T., and Crawford, N. M. (2000) Genomic analysis of a nutrient response in Arabidopsis reveals diverse expression patterns and novel metabolic and potential regulatory genes induced by nitrate. *Plant Cell* **12**, 1491–1509.
6. Arredondo-Peter, R., Hargrove, M. S., Moran, J. F., Sarath, G., and Klucas, R. V. (1998) Plant hemoglobins. *Plant Physiol.* **118**, 1121–1125.
7. Hill, R. D. (1998) What are hemoglobins doing in plants? *Can. J. Bot.* **76**, 707–712.
8. Dordas, C., Rivoal, J., and Hill, R. D. (2003) Plant haemoglobins, nitric oxide and hypoxic stress. *Ann. Bot.* **91** Spec No, 173 – 178.
9. Smagghe, B. J., Trent, J. T., III, and Hargrove, M. S. (2008) NO dioxygenase activity in hemoglobins is ubiquitous in vitro, but limited by reduction in vivo. *PLoS ONE* **3**, e2039.
10. Igamberdiev, A. U., Seregelyes, C., Manach, N., and Hill, R. D. (2004) NADH-dependent metabolism of nitric oxide in alfalfa root cultures expressing barley hemoglobin. *Planta* **219**, 95–102.
11. Perazzolli, M., Dominici, P., Puertas, M. C. R., Zago, E., Zeier, J., Sonoda, M., Lamb, C., and Delledonne, M. (2004) Non-symbiotic hemoglobin AHb1 modulates nitric oxyde bioactivity in *Arabidopsis thaliana*. *Plant Cell* **16**, 2785–2794.

12. Belenghi, B., Romero-Puertas, M. C., Vercammen, D., Brackenier, A., Inze, D., Delledonne, M., and Breusegem, F. V. (2007) Metacaspase activity of *Arabidopsis thaliana* is regulated by S-nitrosylation of a critical cysteine residue. *J. Biol. Chem.* **282**, 1352–1358.
13. Igamberdiev, A. U. and Hill, R. D. (2009) Plant mitochondrial function during anaerobiosis. *Ann. Bot.* **103**, 259–268.
14. Perazzolli, M., Romero-Puertas, M. C., and Delledonne, M. (2006) Modulation of nitric oxide bioactivity by plant haemoglobins. *J. Exp. Bot.* **57**, 479–488.
15. Brunori, M., Giuffre', A., Nienhaus, K., Nienhaus, G. U., Scandurra, F. M., and Vallone, B. (2005) Neuroglobin, nitric oxide, and oxygen: functional pathways and conformational changes. *Proc. Natl. Acad. Sci. USA* **102**, 8483–8488.
16. Abbruzzetti, S., Grandi, E., Bruno, S., Faggiano, S., Spyrakis, F., Mozzarelli, A., Dominici, P., and Viappiani, C. (2007) Ligand migration in non symbiotic hemoglobin AHb1 from *Arabidopsis thaliana*. *J. Phys. Chem. B* **111**, 12582–12590.
17. Bruno, S., Faggiano, S., Spyrakis, F., Mozzarelli, A., Abbruzzetti, S., Grandi, E., Viappiani, C., Feis, A., Mackowiak, S., Smulevich, G., Cacciatori, E., and Dominici, P. (2007) The reactivity with CO of AHb1 and AHb2 from *Arabidopsis thaliana* is controlled by the distal His E7 and internal hydrophobic cavities. *J. Am. Chem. Soc.* **129**, 2880–2889.
18. Bruno, S., Faggiano, S., Spyrakis, F., Mozzarelli, A., Cacciatori, E., Dominici, P., Grandi, E., Abbruzzetti, S., and Viappiani, C. (2007) Different roles of protein dynamics and ligand migration in non-symbiotic hemoglobins AHb1 and AHb2 from *Arabidopsis thaliana*. *Gene* **398**, 224–233.
19. Nienhaus, K., Dominici, P., Astegno, A., Abbruzzetti, S., Viappiani, C., and Nienhaus, G. U. (2010) Ligand migration and binding in non-symbiotic hemoglobins of *Arabidopsis thaliana*. *Biochemistry* **49**, 7448–7458.
20. Faggiano, S., Abbruzzetti, S., Spyrakis, F., Grandi, E., Viappiani, C., Bruno, S., Mozzarelli, A., Cozzini, P., Astegno, A., Dominici, P., Brogioni, S., Feis, A., Smulevich, G., Carrillo, O., Schmidtke, P., Bidon-Chanal, A., and Luque, F. J. (2009) Structural plasticity and functional implications of internal cavities in distal mutants of type 1 non-symbiotic hemoglobin AHb1 from *Arabidopsis thaliana*. *J. Phys. Chem. B* **113**, 16028–16038.
21. Hayashi, A., Suzuki, T., and Shin, M. (1973) An enzymic reduction system for metmyoglobin and methemoglobin, and its application to functional studies of oxygen carriers. *Biochim. Biophys. Acta* **310**, 309–316.
22. Abbruzzetti, S., Sottini, S., Viappiani, C., and Corrie, J. E. T. (2005) Kinetics of proton release after flash photolysis of 1-(2-nitrophenyl)ethyl sulfate (caged sulfate) in aqueous solutions. *J. Am. Chem. Soc.* **127**, 9865–9874.
23. Abbruzzetti, S., Bruno, S., Faggiano, S., Grandi, E., Mozzarelli, A., and Viappiani, C. (2006) Monitoring haem proteins at work with nanosecond laser flash photolysis. *Photochem. Photobiol. Sci.* **5**, 1109–1109.
24. Henry, E. R. and Hofrichter, J. (1992) Singular value decomposition: application to analysis of experimental data. In: Numerical Computer Methods, Vol. **210** (Brand, L., and Johnson, M. L., eds.). pp. 129–192, Academic Press, San Diego.
25. Sottini, S., Abbruzzetti, S., Viappiani, C., Ronda, L., and Mozzarelli, A. (2005) Determination of microscopic rate constants for CO binding and migration in myoglobin encapsulated in silica gels. *J. Phys. Chem. B* **109**, 19523–19528.
26. Nienhaus, K., Kriegl, J. M., and Nienhaus, G. U. (2004) Structural Dynamics in the Active Site of Murine Neuroglobin and Its Effects on Ligand Binding. *J. Biol. Chem.* **279**, 22944–22952.
27. Abbruzzetti, S., Faggiano, S., Bruno, S., Spyrakis, F., Mozzarelli, A., Dewilde, S., Moens, L., and Viappiani, C. (2009) Ligand migration through the internal hydrophobic cavities in human neuroglobin. *Proc. Natl. Acad. Sci. USA* **106**, 18984–18989.
28. Sottini, S., Abbruzzetti, S., Spyrakis, F., Bettati, S., Ronda, L., Mozzarelli, A., and Viappiani, C. (2005) Geminate rebinding in R state hemoglobin: kinetic and computational evidence for multiple hydrophobic pockets. *J. Am. Chem. Soc.* **127**, 17427–17432.
29. Bisht, N. K., Abbruzzetti, S., Uppal, S., Bruno, S., Spyrakis, F., Mozzarelli, A., Viappiani, C., and Kundu, S. (2011) Ligand migration and hexacoordination in type 1 non symbiotic rice hemoglobin. *Biochim. Biophys. Acta – Proteins and Proteomics* **1814**, 1042–1053.
30. Minning, D. M., Gow, A. J., Bonaventura, J., Braun, R., Dewhirst, M., Goldberg, D. E., and Stamler, J. S. (1999) Ascaris haemoglobin is a nitric oxide-activated 'deoxygenase'. *Nature* **401**, 497–502.
31. Jia, L., Bonaventura, C., Bonaventura, J., and Stamler, J. S. (1996) S-Nitrosohaemoglobin: a dynamic activity of blood involved in vascular control. *Nature* **380**, 221–226.
32. Angelo, M., Singel, D. J., and Stamler, J. S. (2006) An S-nitrosothiol (SNO) synthase function of hemoglobin that utilizes nitrite as a substrate. *Proc. Natl. Acad. Sci. USA* **103**, 8366–8371.
33. Isbell, T. S., Sun, C. W., Wu, L. C., Teng, X., Vitturi, D. A., Branch, B. G., Kevil, C. G., Peng, N., Wyss, J. M., Ambalavanan, N., Schwiebert, L., Ren, J., Pawlik, K. M., Renfrow, M. B., Patel, R. P., and Townes, T. M. (2008) SNO-hemoglobin is not essential for red blood cell-dependent hypoxic vasodilation. *Nat. Med.* **14**, 773–777.
34. Angelo, M., Hausladen, A., Singel, D. J., and Stamler, J. S. (2008) Interactions of NO with hemoglobin: from microbes to man. *Methods Enzymol.* **436**, 131–168.